SLAC-PUB-12561
June 2007

NONINVASIVE LASER PROBING OF ULTRASHORT SINGLE ELECTRON BUNCHES FOR ACCELERATOR AND LIGHT SOURCE DEVELOPMENT*

Paul R. Bolton,

Stanford Linear Accelerator Center,

P.O. Box 4349, Stanford University,

Stanford, California 94309, USA.

Companion development of ultrafast electron beam diagnostics capable of noninvasively resolving single bunch detail is essential for the development of high energy, high brightness accelerator facilities and associated beam-based light source applications. Existing conventional accelerators can exhibit timing-jitter down to the 100 femtosecond level which exceeds their single bunch duration capability. At the other extreme, in relatively jitterless environments, laser-plasma wakefield accelerators (LWFA) can generate single electron bunches of duration estimated to be of order 10 femtoseconds making this setting a valuable testbed for development of broadband electron bunch diagnostics. Characteristics of electro-optic schemes and laser-induced reflectance are discussed with emphasis on temporal resolution.

Keywords: accelerator diagnostics; electro-optics; laser-induced reflectance

1. Introduction

Noninvasive, single electron bunch diagnostics that can operate at accelerator repetition rates and are capable of ultrashort temporal resolution are essential for current accelerator and associated light source developments with dense bunches. A good example is the SPPS Facility at SLAC (a predecessor to LCLS) where electron bunches of duration near 80 femtoseconds are generated with approximately 200 femtosecond timing-jitter relative to an external, synchronized laser probe [1]. Similar requirements exist for the XFEL facility at DESY and its TESLA predecessor. Diagnostic requirements are even more demanding for novel all-optical laser wakefield accelerator (LWFA) sources where probe timing-jitter is essentially zero and estimated bunch lengths can be of order 10 femtoseconds [2,3,4].

This report briefly describes known techniques that use synchronized laser probe pulses for diagnosing timing-jitter and individual bunch detail. It also assesses their temporal resolution capabilities. This includes various electro-optic techniques and laser-induced reflectance. Methods employed to measure timing-jitter require an external probe that is synchronized to the accelerator facility (typically to the RF phase). It is critical to evaluate the key features of candidate techniques, to determine optimum parameter values, and to compare with methods that do not require such synchronized probes. Development and control of future electron accelerator and light sources can be limited by the availability of appropriate diagnostics. A new generation of ultrafast electron bunch diagnostics is much needed.

2. Electro-optic Techniques:

Electro-optic methods use the electric field, E_{bunch} of an electron bunch (pump pulse) to induce a birefringence in a laser probe pulse that is coincident with the bunch field as it propagates across an electro-optic crystal. Ellipsometric detection can be used to diagnose the dynamic retardation effect. Independent of the bunch field, static retardation may also exist that is attributed to intrinsic birefringence in the crystal.

2.1. *Electric Field of a Single Electron Bunch*

Submitted to International Journal of Modern Physics B

Work supported by US Department of Energy contract DE-AC02-76SF00515

The electric field of a single electron bunch containing a total charge, Q and with longitudinal scale parameter, σ can be determined according to:

$$E_{bunch} = \frac{1.8x10^{10} Qe^{-\frac{s^2}{2\sigma^2}}}{\sigma R\sqrt{2\pi}} \quad \text{for} \quad \frac{R}{\sigma\gamma} < 1 \qquad (1)$$

where R is the distance from the electron beamline, and s is the longitudinal position within the bunch. At adequately high electron energies, γmc^2 (c is the vacuum light speed) the field direction is predominantly radial (confined to a disk perpendicular to the electron beamline). Field amplitudes can be large enough to induce observable electro-optic effects. For example, with Q of 1 nanoCoulomb, a 30 micron full width at half maximum (FWHM) for the bunch field (for which $\sigma = 12.74$ microns), and a radial distance, R of 5 millimeters from the beamline, the peak bunch field ($s = 0$) is at the MV/cm level.

2.2. *Pockels and Kerr Effects:*

Electro-optical and nonlinear optical effects can be described by expanding the impermeabilty tensor, η_{ij} with respect to the applied field, $\overline{E}$ as follows [5]:

$$\Rightarrow \eta_{ij}\left(\overline{E}\right) = \eta_{ij}^{0} + \sum_{k} r_{ijk}E_k + \sum_{k,l} S_{ijkl}E_kE_l \qquad (2)$$

for which we define:

$$r_{ijk} \equiv \frac{\partial \eta_{ij}}{\partial E_k} \approx \frac{-4\overline{\overline{\overline{d}}}}{\varepsilon_o n_o^4} \quad \text{and} \quad S_{ijkl} \equiv \frac{1}{2}\frac{\partial^2 \eta_{ij}}{\partial E_k \partial E_l} \approx \frac{-12\overline{\overline{\overline{\overline{\chi^{(3)}}}}}}{\varepsilon_o n_o^4} \qquad (3)$$

The Pockels effect (linear electro-optic effect) is represented by the all terms that are linear in the field components, E_k . The Pockels tensor, r_{ijk} contains coefficients for the linear terms. A linear dependence of the impermeability corresponds also to a linear dependence for the refractive index, n . A so-called Pockels medium therefore is not centro-symmetric and cannot be structurally amorphous.

The Kerr effect (quadratic electro-optic effect) is represented by all terms that are quadratic and depend on the field component product, E_kE_l . The Kerr tensor, S_{ijkl} contains coefficients for the quadratic terms. This quadratic dependence of the impermeability establishes a quadratic dependence for the refractive index, n . Consequently, Kerr media are centro-symmetric and include amorphous media.

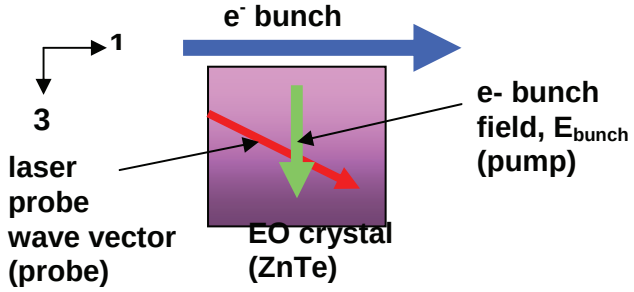

Figure 1. Typical electro-optic configuration for an electron bunch diagnostic.

2.3. *Electro-optic Signal*

Using a ZnTe crystal, for example and with collinear propagation of the electron bunch and laser probe, as shown in figure 1, the Pockels-induced dynamic retardation encoded onto an optical probe due to the Pockels effect is defined to be [5]:

$$\Gamma_{dyn} \equiv \Gamma\left(n_3\left(E_{bunch}\right)\right) - \Gamma\left(n_2\left(E_{bunch}\right)\right) = \pi \frac{E_{bunch}}{E_{\pi p}}$$

$$E_{\pi p} \equiv \frac{\lambda}{L r_{41} n_o^3} \tag{4}$$

where $E_{\pi p}$ is the Pockels field required to induce a phase retardation of π radians in a probe of wavelength, λ within a crystal thickness, L. The zero field refractive index is n_o. The refractive indices in the presence of the bunch field along the principal axes 1 and 3 (see figure 1) are n_1 and n_3 respectively. Crystal symmetry affords specification of the Pockels coefficient r_{ijk} with only two indices. With λ of 800 nm and a ZnTe crystal of 200 micron thickness, $E_{\pi p}$ is approximately 500 kV/cm. Similarly, a Kerr-induced dynamic phase retardation and a Kerr field for a retardation of π radians, $E_{\pi k}$ can be defined. The Pockels transmitted intensity signal is defined here to be:

$$Signal_{\text{int\_ Pockels}} \equiv \left| 1 - \left\{ \frac{\sin^2\left(\frac{\phi_o}{2} - \frac{\pi}{2} \frac{E_{bunch}}{E_{\pi p}} \right)}{\sin^2\left(\frac{\phi_o}{2} \right)} \right\} \right| \tag{5}$$

The use of the Kerr effect can provide purer EO signals (with insignificant Pockels contributions) but generally requires much higher bunch fields. While $Signal_{\text{int\_ Pockels}}$ is about 31 % for $\frac{E_{bunch}}{E_{\pi p}}$ = 10%, a similarly defined $Signal_{\text{int\_ Kerr}}$ is only about 16 % for $\frac{E_{bunch}}{E_{\pi k}}$ = 10% (an optical bias, $\frac{\phi_o}{2}$ of $\frac{\pi}{4}$ is assumed). Lower π fields, $E_{\pi p}$ and $E_{\pi k}$ are preferable and can be obtained with lower wavelength probes. One factor determining the limit to lower wavelength is the onset of absorption in the EO crystal. Two-photon absorption (TPA) can render visible probes unfeasible for bandgaps near 2eV (such as ZnTe). The remainder of this report refers only to signals generated by the Pockels effect.

2.4. Key Issues Limiting Temporal Resolution

Temporal resolution is limited in part by the duration of the laser probe pulse, τ so that $\delta t_{probe} = \tau$ (in the absence of optical detection resolution well beyond this duration) and by geometry (because bunch field lines are not rigorously perpendicular to the electron beamline and have an angular spread near, $\frac{2}{\gamma}$) where $\delta t_{geom} \approx \frac{2R}{\gamma c}$ [6]. For example, for a 1GeV electron beam and separation, R of 5 mm, δt_{geom} is about 17 femtoseconds. Contributions, δt_{probe} and δt_{geom} are minimized using minimum probe pulse durations and distances in addition to maximum beam energy. They are independent of the electro-optic material and probe frequency.

More complex resolution limits for EO detection (for which mitigation efforts can pose a greater challenge) are attributed to frequency-dependent, optical properties of materials. These include variation of Fresnel reflection and transmission at crystal surfaces, variation of electro-optic coefficients, phase

matching requirements of bunch field and optical field mixing, dielectric resonance behaviour, and spectral dispersion in general.

Treating the bunch field-optical field mixing as sum and difference frequency generation in the crystal reduces phase matching in the collinear propagation case to :

$$n_{bunch} = n_{o,group} \Rightarrow v_{o,group} = v_{bunch,phase} \tag{6}$$

The phase velocity of the bunch field, $v_{bunch,phase}$ is matched to the group velocity of the laser probe, $v_{o,group}$ (for the noncollinear case where the probe propagates inside the crystal at a refracted angle θ with respect to the surface normal , use $\frac{n_{o,group}}{\cos\theta}$ instead of $n_{o,group}$). One can envision in the mismatched case, a temporal slippage or 'smearing' of the bunch field relative to the probe field that results in the following estimated (for rectangular longitudinal pulse profiles) nonresonant phase mismatching contribution to the temporal resolution that is achievable with the EO methods:

$$\begin{aligned} \frac{L}{c} n_{bunch} \rho(1-\rho) &= \frac{L}{c} \rho \Delta n \equiv \delta t_{nonresphase} \\ \Delta n &\equiv n_{bunch} - n_{o,group} \\ \rho &\equiv \frac{n_{o,group}}{n_{bunch}} \end{aligned} \tag{7}$$

For a ZnTe crystal thickness, L of 500 microns and a probe central wavelength of 800 nm, $\delta t_{nonresphase}$ is about 480 femtoseconds (using $n_{bunch} \approx 3.18$ and $n_{o,group} \approx 2.85$). Although this contribution can be reduced by reducing the thickness of a given crystal this is done at the cost of signal level. It is important to minimize Δn prior to any thickness reduction. Resonances enhance spectral dispersion (normal and abnormal types) and reduce bunch field amplitude with propagation across a crystal. Consider ω_{bunch} to be a frequency component of the electron bunch field. According to the classical oscillating electron model of dielectric resonance, the frequency dependent refractive index, $n(\omega_{bunch})$ in the vicinity of resonant frequency, $\omega_{o,THz}$ is expressed simply as:

$$\Rightarrow n(\omega_{bunch}) \approx n_o + \frac{\chi_0 \omega_{o,THz}}{4 n_o} \left(\frac{\omega_{o,THz} - \omega_{bunch}}{(\omega_{o,THz} - \omega_{bunch})^2 + \left(\frac{\Delta\omega_{THz}}{2}\right)^2} \right) \tag{8}$$

where χ_o is the susceptibility attributed to the resonance, $\Delta\omega_{THz}$ is the absorption bandwidth (it also marks the interval of abnormal dispersion of the refractive index from $\omega_{o,THz} - \frac{\Delta\omega_{THz}}{2}$ to $\omega_{o,THz} + \frac{\Delta\omega_{THz}}{2}$), and n_o is the static refractive index. A similar result can be given for ω_{bunch} dependent extinction. Although the effects of a single dielectric resonance may be calculable, the resonance degrades phase matching in general, introducing ambiguity in the determination of amplitude and

longitudinal profiles of the bunch field. This is because dispersive and absorptive effects are not temporally resolved but are integrated internally across the crystal prior to detection. The presence of multiple resonances further complicates these effects. In ZnTe for example, there is a strong transverse-optical-phonon resonance at 5.34 THz, a weaker transverse-acoustic-phonon resonance at 3.7 THz and another weaker longitudinal-acoustic-phonon resonance at 1.6 THz [7]. Results in Ref. 7 have shown that for a ZnTe crystal of 100 micron thickness the 4.35 THz spectral cutoff of the filter function amplitude (representing a temporal resolution near 230 femtoseconds) is attributed to the degraded phase matching. It is clearly desirable for the bunch field spectrum to be well below $\omega_{o,THz} - \frac{\Delta\omega_{THz}}{2}$ for any significant resonances. The spectra of ultrashort electron bunch fields can extend well above resonant frequencies (for example 12 femtosecond ir laser pulses are known to generate THz pulses with spectral components up to 30 THz [8]) and intrinsic material properties establish critical limits for temporal resolution. Total phase mismatch contributions that include resonance effects are denoted as δt_{phase} (which must be greater than $\delta t_{nonresphase}$ according to its definition).

2.5. Types of Electro-optic Schemes

2.5.1 Spectral -Temporal Transcription

Spectral-temporal transcription is achieved in a synchronous chirped laser probe pulse that propagates coincidentally with the bunch field across the crystal as illustrated in the crossed-polarizer configuration of figure 2 [6,9]. Frequency chirp establishes a correlation between time and instantaneous frequency within the probe waveform. A suitably 'stretched' probe also facilitates overlap with the bunch field, given that there can be significant timing-jitter between the electron bunch and probe at the crystal site. As seen in figure 2, an optical bias allows measurement of 'S' and 'P' polarization transmission whose energy balance is interrupted by the dynamic retardation. This effect is revealed in the integrated, transmitted spectra. The following contributions to temporal resolution have been estimated with the single electron bunch diagnostic application reported in Ref. 6: $\delta t_{geom} \approx 75$ femtoseconds, $\delta t_{spect} \approx 300$ femtoseconds,

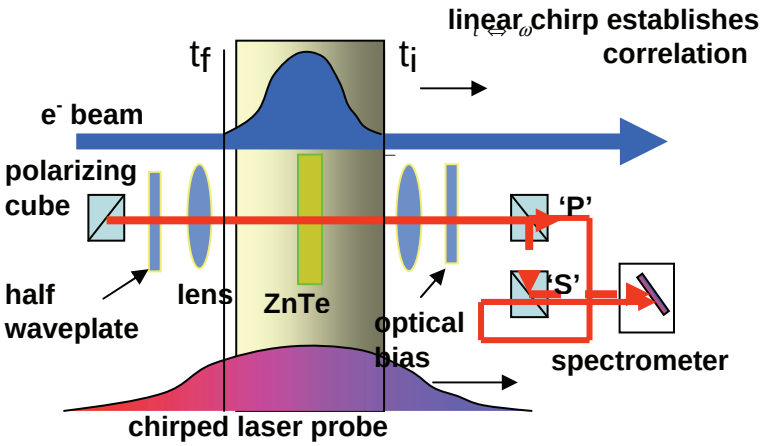

Figure 2. Basic EO configuration for spectral-temporal transcription scheme.

$\delta t_{nonresphase} \approx 480$ femtoseconds, and $\delta t_{transform} \approx 370$ femtoseconds. The δt_{spect} contribution is due to the spectral resolution limit. For an ultrashort electron bunch field we can reach a limit where the Fourier

spectral width equals that attributed to the probe chirp over this interval. This limiting interval, $\delta t_{transform} = \tau_o \sqrt{\frac{\tau_{probe}}{\tau_o}}$ is unique to this EO method [10]. τ_o is the transform limited probe duration.

Another unique limitation of this technique is with the interpretation of the spectral signal. Defining the transmitted probe field signal (in the 'S' or 'P' channel) as a linear modulation of the incident probe field by the electron bunch field, the integrated spectral signals are modulations of the incident probe spectrum (centered at frequency ω_o) by a factor that is not simply the bunch field alone but instead the bunch field convolved with a resolution function, $G(t, \omega - \omega_o)$ (which depends on the probe field) according to [11]:

$$Spectral\_Signal\_Intensity \approx 2\beta \left| \tilde{E}_{probe}(\omega) \right|^2 \left\{ E_{THz}(t') \otimes \mathrm{Re}(G(t, \omega - \omega_o)) \right\} \quad (9)$$

This result accounts for the generation of sidebands associated with bunch field modulation. Sidebands become increasingly important for ultrashort electron bunches; especially where they can spectrally exceed the extent of the incident probe spectrum. It can be more appropriate, in these cases, to address spectral dynamics in the EO signal and to consider diagnostics that can provide this kind of information (such as SPIDER or FROG as is discussed later in this report) [12,13].

How to minimize δt_{geom} and δt_{spect} resolution contributions is relatively clear. The transform contribution, $\delta t_{transform}$ can be reduced below the 70 femtosecond level by using use broader band probe pulses for which τ_o < 5 femtoseconds[6]. The dominant contributions to temporal resolution that remain are due to resonances and related phase mismatching, δt_{phase} (i.e. frequency dependent EO material limits) Reduction to the 100 femtosecond level is a major challenge. For a ZnTe crystal of 100 micron thickness, δt_{phase} is still about 230 femtoseconds [7]. Note that in ZnTe with an 800 nm probe, even the nonresonant contribution, $\delta t_{nonresphase}$ (as defined above) is about 100 femtoseconds for this small thickness.

2.5.2. Direct - Temporal Transcription

Direct, ultrafast detection of the transmitted waveform exiting the crystal (as opposed to using time-integrated spectra) can be used to avoid troublesome issues associated with spectral-temporal transcription. It is referred to as direct-temporal transcription for which there are no contributions to temporal resolution from δt_{spect} and $\delta t_{transform}$. Because a spectral-temporal correlation is not used the probe pulse can remain chirped but only to the extent needed to achieve reliable pulse-to-pulse overlap with an electron bunch with timing-jitter considered.

2.5.2a Cross-Correlation Detection

Jamison et al developed the direct-transcription scheme using cross-correlation of the transmitted probe with a known ultrashort reference pulse [11]. In this work, a crossed-polarizer configuration was used to measure an EO intensity signal of duration 450 femtoseconds (i.e. bias, ϕ_o = 0)[14]. The δt_{geom} contribution to temporal resolution was about 75 femtoseconds (methods to further reduce this have been mentioned above). In addition to the δt_{probe} contribution of 30 femtoseconds, cross-correlator detection introduces a typical contribution to temporal resolution due to the spatial resolution of imaged second harmonic light (SHG) that is used as the correlated signal, $\delta t_{SHGcorrel}$ and this has been estimated to be near 50 femtoseconds. The dominant contribution to temporal resolution is still attributed to material resonance and related phase mismatching. For the ZnTe crystal of 500 micron thickness that was used, it was estimated that the spectral components of the bunch field below about 2.8 THz could be detected with minimal distortion suggesting a 360 femtosecond material limit to resolution[14]. For this thickness in ZnTe,

the nonresonant phase mismatch component (i.e. based on index mismatch alone) is about 480 femtoseconds.

2.5.2b FROG Detection (FROGEO)

A more complete diagnostic for direct-temporal transcription is one that combines high temporal and spectral resolution of the signal waveform transmitted through the EO crystal. An example is the well-known frequency-resolved optical-gating technique (FROG)[15]. The FROG technique is based on iterative analysis of a 2D FROG trace or spectrogram which fundamentally includes autocorrelation for any spectral component. Several versions of FROG have been developed by Trebino and his colleagues[16]. In the polarization-gated version (PG-FROG) optical gating is achieved via the Kerr effect in an amorphous material. The signal field (intensity) associated with the 2D trace scales cubically (to the sixth power) with the field of the incident waveform to be analyzed according to:

$$I_{frog}(\omega,\tau) \propto \left| \int_{-\infty}^{\infty} E(t)\left|E(t-\tau)\right|^2 \exp(-\imath\omega t)dt \right|^2 \qquad (10)$$

Consequently, PG-FROG is sensitive to temporal asymmetry in the field envelope of the waveform. This is essential for typical bunch fields that may have very different rise and fall times in addition to other bunch asymmetry. As seen in figure 3, a FROG diagnostic can be naturally integrated into an electro-optic setup. This combined EO plus FROG configuration is referred to as 'FROGEO'. Some key advantages of FROGEO are now mentioned. The FROG diagnostic is robust (the PG version in particular). With the addition of polarizing optics, polarization extinction for EO ellipsometry is improved. Analysis of the 2D FROG trace uniquely determines the phase and field amplitude history for a single ultrashort EO waveform and therefore isolates effects of a single electron bunch field. Because bandwidth determination is intrinsic to FROG, lower probe pulse bandwidths, that are better behaved in transport to an EO site, can be used in FROGEO (as with the cross-correlation scheme, one only requires a chirped probe whose duration is adequate to incorporate pulse-to-pulse timing-jitter). If an ultrashort broadband probe were used (for example, in a case for which timing-jitter is negligible) FROGEO provides a pulse-to-pulse monitor of the dispersed probe duration that exits the EO crystal with temporal resolution of order 10 femtoseconds (δt_{probe} is no longer a probe limit). So, 2D FROG traces can better deal with longitudinal probe 'shaping'.

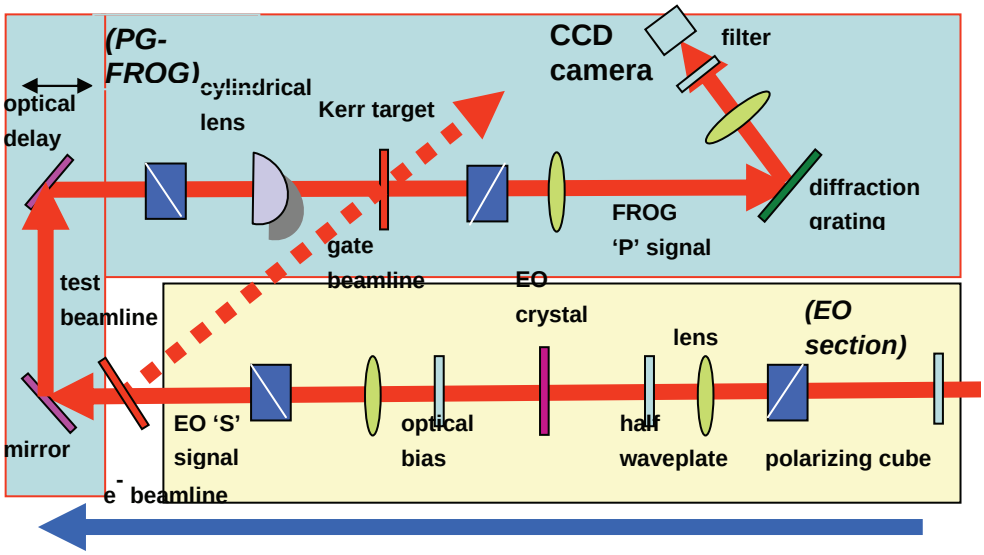

Figure 3. Integrated FROGEO configuration.

Finally, the FROGEO scheme intrinsically monitors the spectral dynamics that may be critical for

diagnosing ultrashort electron bunches. Mindful of ultrashort electron bunch fields, spectral dynamics reveal the time-dependent development of spectral sidebands on a narrower band probe waveform and are also sensitive to refractive index dynamics[12,13]. This feature might also prove valuable for distinguishing bunch wakefields which can be of high amplitude but dynamically slower than the bunch field itself. This novel use of spectral dynamics clearly favours the use of incident probe pulses of minimal bandwidth in order to expose dynamics that are 'out-of-band'.

A disadvantage of FROGEO is the single pulse energy requirement. For example, with 2D trace detection by an n-bit camera and with inefficient third order diffraction from a reflective optical grating, the ir PG-FROG detector developed at SSRL's Gun Test Facility at SLAC requires single pulse energy that is estimated to be:

$$\left(\varepsilon_{\min}\right)^3 \propto \frac{16\left(\Delta t \Delta\lambda\right)}{2^n} \tag{11}$$

where the units are microjoules for $\varepsilon_{\min}$, nanometers for $\Delta\lambda$, and femtoseconds for Δt.

Although FROGEO may be best implemented in the linear small signal regime with an optical bias, ϕ_o of zero, it has been established in Lab2 simulations that the 2D FROG trace uniquely reveals the effects of an ultrashort EO induced waveform superimposed on a longer probe pulse background [17]. It is important to note that, although an ultrafast diagnostic that is used to detect (with highest temporal resolution) the transmitted waveform for direct-temporal transcription cannot resolve the effects of resonance and phase mismatching (that accumulate during coincident propagation across the crystal), one can use multiple crystals of different thicknesses at a single EO site to evaluate the effect and significance of absorption and /or 'smearing' (time slippage) due to refractive index differences.

2.5.3. Spatial-Temporal Transcription

A spatial-temporal transcription can be established when the laser probe pulse is of nonnormal incidence [18]. Figure 4 illustrates the geometry at the crystal where the probe incident angle is ϕ with respect to the crystal surface. At the exit surface of the crystal (imaged with magnification, M) there exists a correlation between spatial extent across the probe transverse profile (along the dimension perpendicular to the plane of incidence) and the arrival time of the probe at the crystal. Geometry determines the spatial scan duration, δt_{scan} and the scan rate, $\frac{D}{\delta t_{scan}}$ to be:

$$\delta t_{scan} = \frac{d}{c\tan\phi} \quad \text{and} \quad \frac{D}{\delta t_{scan}} \equiv \frac{c}{\cos\phi} \tag{12}$$

Typical scan rates are at the mm/picosecond level with the single pixel time interval, δt_{pixel} being only a few femtoseconds (much less than δt_{probe}). The remaining configuration for EO ellipsometry (not shown) is similar to that shown in figure 2. The probe pulse spotsize, d can be as large as needed to set the desired scan time, within a given crystal size, (which must be large enough to incorporate timing-jitter between the probe and the electron bunch) and the probe duration, δt_{probe} which is the integration interval for each pixel in the image should be as short as possible. These probe attributes are essentially the opposite of those required in a spectral-temporal transcription scheme. Temporal resolution is limited by the probe duration, δt_{probe}, the usual geometric term, δt_{geom}, an imaging resolution term, $\delta t_{image} \equiv m\delta t_{pixel}$, a probe diffraction term, $\delta t_{diff} \approx 29\sqrt{L}$, and by the dominant resonance/phase mismatch term, δt_{phase}. At SLAC's SPPS facility, Cavalieri et al have demonstrated the application of this technique to monitoring timing jitter at the 200 femtosecond level between an ir laser probe and an electron bunch [1]. In this work,

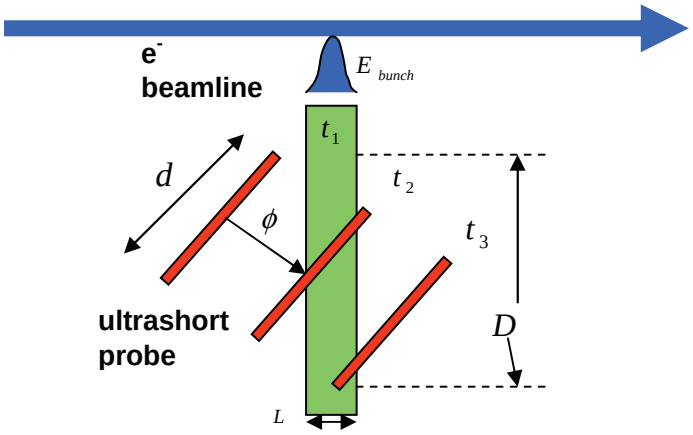

Figure 4. 'Tilted' incidence for spatial-temporal transcription scheme.

$\phi = 45$ degrees, $\delta t_{scan} \approx 9$ picoseconds, $\delta t_{probe} \approx 135$ femtoseconds , $\delta t_{geom} \approx 1$ femtosecond, $\delta t_{diff} \approx 10$ femtoseconds , and $\delta t_{nonresphase} \approx 140$ femtoseconds (and the spectral cutoff of the filter function using a ZnTe crystal of 200 micron thickness is near 4 THz such that $\delta t_{phase} \approx 250$ femtoseconds [6]). The bunch field scales with R^{-1} , and because large spotsizes are required for the spatial-temporal technique the spatial uniformity of the bunch field is a greater issue. Bunch field nonuniformity across the total scan distance, D of figure 4 can be kept relatively small if $\frac{d}{D\sin\phi} << 1$ for materials with high refractive indices like ZnTe. Finally, given the significantly nonuniform spatial profile that is anticipated for the transmitted probe, a FROGEO version of the spatial-temporal transcription technique is not feasible.

3. Laser-Induced Reflectance (LIR)

An electron bunch diagnostic in which the roles of pump and probe (relative to EO techniques discussed so far) are reversed is based on laser-induced reflectance in semiconductors (LIR). Laser-induced carrier excitation in a semiconductor (silicon in this example) establishes a highly localized electron-hole plasma which can significantly alter (and thereby control) the refractive index in the regime of THz frequencies. The LIR technique is well known as a method for gated switching (reflection) of THz radiation[19,20,21]. According to the Drude model, the modified, complex dielectric function, ε_{Drude} for the induced electron-hole plasma can be expressed as:

$$\varepsilon_{Drude}(\omega_b,t) = \varepsilon_o - \frac{n_{eh}(t)}{1+c^2(\omega_b,t)}\left(\frac{1}{n_{e,crit}(\omega_b)}+\frac{1}{n_{h.crit}(\omega_b)}\right) - \imath\frac{n_{eh}(t)c(\omega_b,t)}{1+c^2(\omega_b,t)}\left(\frac{1}{n_{e,crit}(\omega_b)}+\frac{1}{n_{h.crit}(\omega_b)}\right) \quad (13)$$

$$c(\omega_b,t) \equiv collisionality$$

where ε_o is the real intrinsic permittivity of the semiconductor, $n_{eh}(t)$ is the time-dependent electron-hole density, and $n_{e,crit}(\omega_b)$ and $n_{h,crit}(\omega_b)$ are THz frequency-dependent critical densities for electrons and holes respectively. Dielectric function dynamics establishes Fresnel reflectance and transmittance dynamics. Computed results of Figure 5 show the reflectance alteration induced by an 800 nm laser pulse

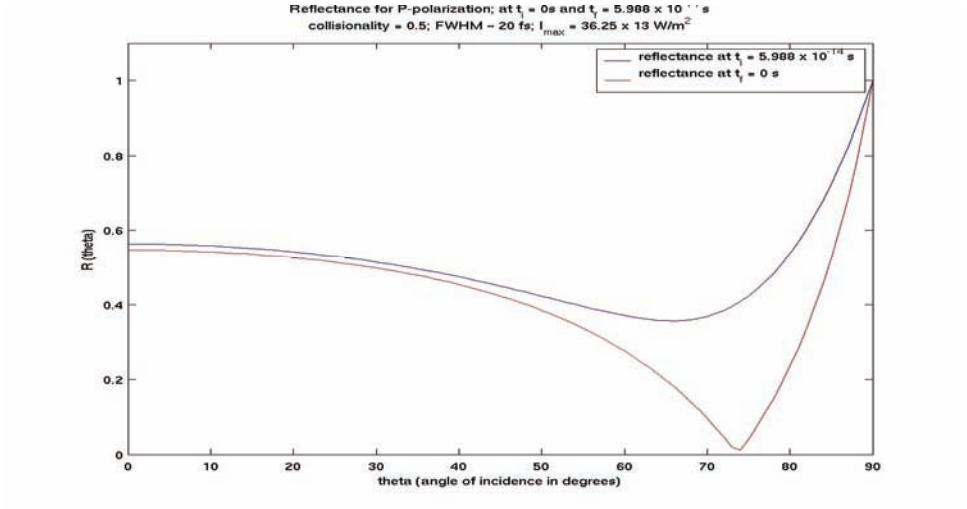

Figure 5. Brewster-like switching action of LIR.

of 20 femtosecond duration, focused to a 2.5 mm spotsize at normal incidence onto a silicon surface[22]. Results are shown for 'P' polarized, 1 THz probe incident at the initial Brewster angle of 74 degrees. A collisionality of 0.5 was assumed. The upper curve represents the enhanced reflectance immediately following the laser pump. A Brewster-like 'switching' action is observed (when compared to the lower curve without the pump) wherein the Brewster angle is abruptly reduced (the nonzero collisionality is responsible for the new reflectance minimum not being zero). At the 74 degree incident angle the probe reflectance is increased from near zero to about 35 % within 40 femtoseconds. Note that the excited carrier relaxation time in the semiconductor is much longer than the pump and probe pulse durations (or order nanoseconds). One can envision a configuration of two orthogonal grazing incidence planes that establish time slews; one for the laser pump and the other for the THz probe. A THz image of the reflected THz light reveals an illuminated region that shifts laterally according to the timing jitter between the two pulses. The main contribution to temporal resolution is δt_{probe} (δt_{image} is expected to be much smaller). Like EO spatial-temporal transcription, imaged signals are integrated over the probe duration. However, because this is diagnostic is based on reflection, it is anticipated that δt_{phase} would be relatively insignificant and that frequency-dependent material properties no longer play a major role. Implementing high resolution LIR depends critically on dispersion compensated transport to the diagnostic site in order to maintain an ultrashort pump pulse. Where the THz probe is generated by an electron bunch, this LIR setup is a relatively simple one that is well suited to timing-jitter assessment.

4. Summary

It is appropriate to consider the diagnostic pair in which one component measures timing-jitter (typically on the coarser time scale) and the other measures single bunch detail. LIR and the EO spatial-temporal transcription techniques show promise for timing-jitter assessment. Both techniques share the same δt_{probe} based resolution limits and concerns. For example, for jitter measurements, it is desirable that $\delta t_{probe} < 50$ femtoseconds. For LIR, incident laser fluences level must be well below surface and bulk material damage thresholds. Because the laser probe must be transmitted through the EO crystal, the dominant contribution for the latter technique is δt_{phase} , which can exceed 100 femtosconds (even for a ZnTe crystal of only 50 micron thickness).

Of the EO techniques discussed here, FROGEO and spatial-temporal transcription are noteworthy for measuring single bunch detail. Although both share the dominant δt_{phase} resolution limit, FROGEO can provide transmitted probe detection with resolution well below δt_{probe} (allowing use of narrower bandwidth probes that are less dispersive) and affords novel use of spectral dynamics for single bunch

measurement which may become critical for the extreme ultrashort cases such as those generated in LWFA schemes. With shortest possible δt_{probe} values (for example, < 10 femtoseconds) LIR also holds promise for single bunch measurement because the δt_{phase} contribution to temporal resolution is minimized in reflection.

The state-of-the-art for temporal resolution must be improved and ideally with novel diagnostics that can be integrated into the development and design of new accelerator and light source facilities. Laser–plasma wakefield sources and other types of laser accelerators may be good test bed sites for such diagnostic development where the environment is relatively jitterless, e- beam access can be improved over that for conventional RF accelerators, and where synchronized probes can be more accessible.

* Work supported in part by the DOE Contract DE-AC02-76SF00515.
This work was performed in support of the LCLS project at SLAC.

References

1. A.L. Cavalieri et al., Phys. Rev. Lett. 94, 114801 (2005).
2. S.P.D. Mangles et al., Nature 431, 535 (September 2004).
3. C. G. R. Geddes et al., Nature 431, 538 (September 2004).
4. J. Faure et al., Nature 431, 541 (September 2004).
5. B. E. A. Saleh and M. C. Teich, *Fundamentals of Photonics, Chapter 18* (John Wiley & Sons, 1991).
6. I. Wilke et al., Phys. Rev. Lett. 88[12],124801 (March 2002).
7. G. Gallot et al., Appl. Phys. Lett. 74[23], 3450 (June 1999).
8. H. J. Bakker et al., J.O.S.A B15[6], 1795 (June 1998).
9. Z. Jiang and X.-C. Zhang, Appl. Phys. Lett. 72[16], 1945 (April 1998).
10. F. G. Sun et al., Appl. Phys. Lett. 73[16], 2233 (October 1998).
11. S. P. Jamison et al., Opt. Lett. 28[18], 1710 (September 2003).
12. P.R. Bolton et al., Nucl. Inst. and Meth. in Phys. Res. A507, 220 (2003).
13. P.R. Bolton et al., J.O.S.A B13[2], 336 (February 1996).
14. G. Berden et al., Phys. Rev. Lett. 93[11], 114802 (September 2004).
15. D. J. Kane and R. Trebino, Opt. Lett. 18[10], 823 (May 1993).
16. K. W. DeLong et al., J.O.S.A. B11[9], 1595 (September 1994).
17. H. Schlarb and S. Dusterer, private communication.
18. J. Shan et al., Opt. Lett. 25[6], 426 (March 2000).
19. P. B. Corkum and D. Keith, J.O.S.A B2[12], 1873 (December 1985).
20. T. Nozokido et al., Elect. and Comm. in Japan, Part 2 80[6], 259 (June 1997).
21. R. Ascazubi et al., CLEO Poster presentation (May 16-21, 2004).
22. R. Nanguneri, private communication.